Catalysis Communications 87 (2016) 53–56

Contents lists available at ScienceDirect

Catalysis Communications

journal homepage: www.elsevier.com/locate/catcom

Short communication

Direct catalytic decomposition of nitrous oxide gas over rhodium supported on lanthanum silicate

Naoyoshi Nunotani, Ryosuke Nagai, Nobuhito Imanaka *

Department of Applied Chemistry, Faculty of Engineering, Osaka University,2-1 Yamadaoka, Suita, Osaka, 565-0871, Japan

ARTICLE INFO

Article history:
Received 9 May 2016
Received in revised form 14 July 2016
Accepted 20 August 2016
Available online 21 August 2016

Keywords:
Nitrous oxide
Apatite-type
Lanthanum silicate
Catalyst

ABSTRACT

The environmental impacts of nitrous oxide (N_2O) have received much attention, including contributions to the greenhouse effect and ozone depletion. Currently, the direct catalytic decomposition of N_2O is considered to be the simplest and most promising method for N_2O abatement. In this study, we focused on the high activity of rhodium and the oxide-ion conducting property of lanthanum silicate and prepared novel $Rh/La_{10}Si_{6-x}Fe_xO_{27-\delta}$ catalysts. From the results of catalytic N_2O decomposition activities, $Rh/La_{10}Si_{6-x}Fe_xO_{27-\delta}$ ($x = 1.0$) exhibited the highest catalytic activity and N_2O was completely decomposed at 600 °C.

1. Introduction

Nitrous oxide (N_2O) is a highly potent greenhouse gas with an atmospheric lifetime of 150 years, and its warming effect is ca. 300 times higher than that of carbon dioxide [1]. In addition, N_2O causes stratospheric ozone layer depletion, similar to that caused by chlorofluorocarbons [2]. Since the main industrial sources of N_2O emissions are manufacturing plants of adipic and nitric acid, end-of-pipe treatment is necessary from the viewpoint of reducing global warming and ozone depletion.

To date, several N_2O removal methods have been proposed such as thermal decomposition [3,4], selective catalytic reduction (SCR) [5–7], and direct catalytic decomposition [8–21]. In particular, the direct decomposition of N_2O into N_2 and O_2 is an optimal route for N_2O abatement because the required temperature is lower than that of thermal decomposition (over 800 °C) [4] and there is no need for reducing additives such as ammonia and urea. Rh-based catalysts [8,9], zeolites [10–12], hexaaluminates [13–15], perovskites [16–18], and spinels [19–21] have been reported to exhibit high activities for direct N_2O decomposition.

The mechanism of direct N_2O decomposition was suggested as shown in the following steps [22–25]. In the first step, N_2O gas is adsorbed on the catalytic active site (*):

$$N_2O(g) + {}^* \rightarrow N_2O^* \quad (1)$$

where N_2O^* is adsorbed N_2O on an active site. Subsequently, the N_2O^* is decomposed to N_2 gas and adsorbed oxygen (O^*):

$$N_2O^* \rightarrow N_2(g) + O^* \quad (2)$$

Finally, the O^* is removed by reaction with a N_2O molecule (Eq. (3)) or combination of two close O^* (Eq. (4)), and thereby, the catalytic active site is regenerated:

$$O^* + N_2O(g) \rightarrow N_2(g) + O_2(g) + {}^* \quad (3)$$

$$2O^* \rightarrow O_2(g) + 2^* \quad (4)$$

In this mechanism, the removal of the adsorbed oxygen (Eqs. (3) and (4)) is the rate determining step and the residual O^* in the active sites prevents further N_2O adsorption.

In this study, we focused on an oxide-ion conducting solid to facilitate adsorbed oxygen removal by supplying an oxide ion from the crystal lattice for catalyzing effective N_2O decomposition. Hence, we selected $La_{10}Si_6O_{27}$ (LS) solid as an oxide-ion conducting promoter. LS has a hexagonal ($P6_3/m$) apatite-type structure with an oxide-ion conducting pathway along the *c*-axis [26,27]. Therefore, by combining the LS promoter and a Rh catalyst that has N_2O decomposition activity [8,9], Rh-supported on $La_{10}Si_6O_{27}$ (Rh/LS) was developed and its catalytic activity was investigated. For further enhancing catalytic activity, the Si^{4+} ion sites in the apatite-type LS solid were partially substituted with larger ionic-size and lower-valent Fe^{3+} (ionic radius: 0.063 nm) [28] relative to Si^{4+} (0.040 nm) [28]. This substitution caused an expansion of the lattice size and formation of oxide-ion vacancies for ion migration. Since iron is expected to show two types of valence states

* Corresponding author.
E-mail address: imanaka@chem.eng.osaka-u.ac.jp (N. Imanaka).

http://dx.doi.org/10.1016/j.catcom.2016.08.032
1566-7367/

(+3 and +2), enhancement in oxygen release properties due to the redox chemistry of iron was expected. From this concept, Rh-supported on $La_{10}Si_{6-x}Fe_xO_{27-\delta}$ (Rh/LSF*x*) was synthesized and the N_2O decomposition properties were investigated.

2. Experimental

The apatite-type $La_{10}Si_{6-x}Fe_xO_{27-\delta}$ (LSF*x*) solids were prepared by a sol-gel method. Rh was loaded on the LSF*x* solids by impregnation. After impregnation, the powders were calcined at 600 °C to obtain 1 wt% Rh/LSF*x*. For comparison, a 1 wt% Rh/La_2O_3 (Rh/La_2O_3) sample was also synthesized by the same methods.

The LSF*x* samples were identified by X-ray powder diffraction (XRD). The AC conductivity (σ) was measured by a complex impedance method. After Rh was loaded, the N_2O decomposition reaction were carried out in a conventional fixed-bed flow reactor with a feed gas mixture of 0.5 vol% N_2O–99.5 vol% He. The gas composition was analyzed using a gas chromatograph, and the catalytic activity was evaluated in terms of N_2O conversion. The experimental details are given in the Supplementary Material.

3. Results

The XRD patterns of the LSF*x* solids are presented in Fig. 1. The samples with $x \le 1.0$ have single phase hexagonal apatite-type structures, whereas LSF1.3 is a two-phase mixture of an apatite-type oxide and $LaFeO_3$. Fig. 2 shows the lattice parameters (*a* and *c*) of the apatite-type phase in the prepared samples. In the compositional region that holds a single phase of the apatite-type structure ($x \le 1.0$), both *a* and *c* almost linearly increased with increasing Fe content (*x*) due to the replacement of Si^{4+} ions (ionic radius: 0.040 nm) [28] in LS with larger Fe^{3+} ions (0.063 nm) [28]. When the Fe content (*x*) was above 1.0, the lattice parameters of the apatite-type phase had almost the same values as those of LSF1.0, indicating that the solid solubility limit composition of the apatite-type structure is LSF1.0.

Fig. 3 presents the compositional dependence of the AC conductivity at 600 °C for LSF*x* solids. The conductivity increased with increasing Fe content (*x*), and the highest conductivity was obtained for the solid solubility limit composition (LSF1.0). On the contrary, LSF1.3 with a two-phase mixture exhibited low conductivity compared to that of LSF1.0. The origins of such change are discussed in Section 4.

For Rh-supported on LSF*x* catalysts, the compositions measured by X-ray fluorescence analysis were in good agreement with their stoichiometric values within experimental error (Table S1), while the phase of

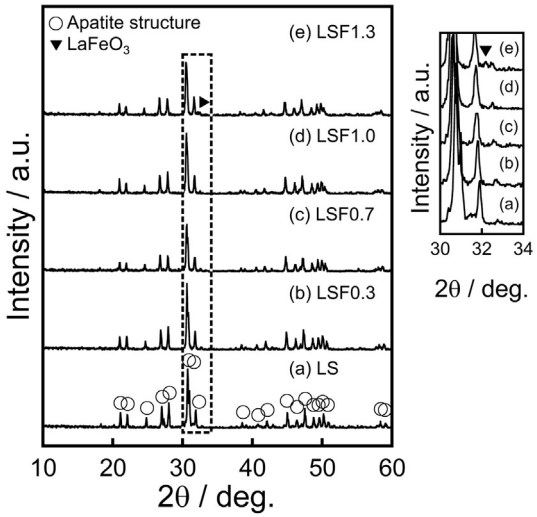

Fig. 1. XRD patterns of the LSF*x* solids.

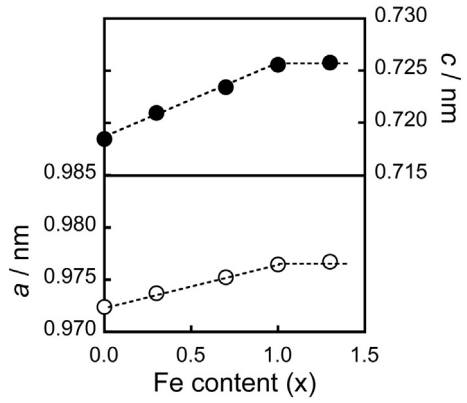

Fig. 2. Compositional dependencies of the lattice parameters (*a* and *c*) of apatite-type phase in the LSF*x* solids.

the Rh could not be identified by XRD measurements owing to its low content. From X-ray photoelectron spectroscopy results shown in Fig. S1, the oxidation states of surface Rh in Rh/LS and Rh/LSF1.0 were confirmed to be trivalent Rh^{3+} [29]. In addition, the valence state of Fe in Rh/LSF1.0 was assigned to be trivalent Fe^{3+} [30–32] (Fig. S2). From the scanning electron microscopy observations of Rh/LS and Rh/LSF1.0 (Fig. S3), the particles formed aggregates and their sizes were not so different between Rh/LS (3.4 μm) and Rh/LSF1.0 (4.3 μm). The Brunauer–Emmett–Teller (BET) specific surface areas of Rh/LSF*x* catalysts, shown in Table S1, were almost the same and had small values of ca. 4 $m^2 \cdot g^{-1}$ owing to the high-temperature calcination of LSF*x* promoters at 1000 °C.

Fig. 4 shows the temperature dependence of N_2O conversion in the Rh/LSF*x* catalysts for comparison with the result of the Rh/La_2O_3; La_2O_3 contains the main elements (La and O) of $La_{10}Si_6O_{27}$ and showed a low AC conductivity ($\sigma < 10^{-7}$ $S \cdot cm^{-1}$ at 600 °C). Regardless of low surface area of Rh/LS (4.3 $m^2 \cdot g^{-1}$) compared to that of Rh/La_2O_3 (10.8 $m^2 \cdot g^{-1}$), the N_2O conversion activity for Rh/LS was significantly enhanced compared to that for Rh/La_2O_3; for instance, the N_2O conversions at 600 °C for Rh/LS and Rh/La_2O_3 were 91.9% and 69.5%, respectively. For the Rh/LSF*x* catalysts with $x \le 1.0$, where LSF*x* promoters hold the single phase, the N_2O conversion activity further increased with increasing Fe content (*x*). The highest activity was obtained for Rh/LSF1.0, and the N_2O was completely decomposed at 600 °C. Here, the formation of neither NO nor NO_2 were detected at 600 °C. In addition, Rh/LSF1.0 exhibited high resistance to O_2, CO_2, and H_2O coexistence (Fig. S4). The reaction mechanism of N_2O decomposition and the effect of Fe in these catalysts are discussed in the next section.

To characterize the oxygen release properties, TPR profiles using hydrogen were measured and the results of Rh/LSF1.0, Rh/LS, and Rh/La_2O_3 are shown in Fig. 5. The reduction temperatures of Rh/LS and

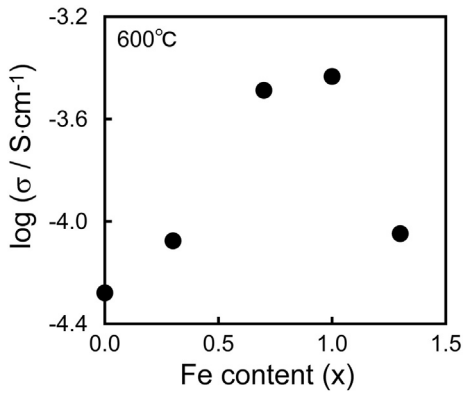

Fig. 3. Compositional dependency of the AC conductivity of the LSF*x* solids.